ACS APPLIED MATERIALS & INTERFACES

Research Article

www.acsami.org

Hierarchical Configuration of $NiCo_2S_4$ Nanotube@Ni–Mn Layered Double Hydroxide Arrays/Three-Dimensional Graphene Sponge as Electrode Materials for High-Capacitance Supercapacitors

Houzhao Wan,[†,‡] Jia Liu,[†] Yunjun Ruan,[†] Lin Lv,[†] Lu Peng,[†] Xiao Ji,[†] Ling Miao,[†] and Jianjun Jiang*[,†]

[†]School of Optical and Electronic Information, Huazhong University of Science and Technology, Wuhan 430074, China

[‡]Hubei Collaborative Innovation Center for Advanced Organic Chemical Materials, Faculty of Physics and Electronic Science, Hubei University, Wuhan 430062, China

Supporting Information

ABSTRACT: Three dimensional (3D) hierarchical network configurations are composed of $NiCo_2S_4$ nanotube @Ni–Mn layered double hydroxide (LDH) arrays in situ grown on graphene sponge. The 3D graphene sponge with robust hierarchical porosity suitable for as a basal growth has been obtained from a colloidal dispersion of graphene oxide using a simple directional freeze-drying technique. The high conductive $NiCo_2S_4$ nanotube arrays grown on 3D graphene shows excellent pseudocapacity and good conductive support for high-performance Ni–Mn LDH. The 3D $NiCo_2S_4$@Ni–Mn LDH/GS shows a high specific capacitance (C_{sp}) 1740 mF cm^{-2} at 1 mA cm^{-2}, even at 10 mA cm^{-2}, 1267.9 mF cm^{-2} maintained. This high-performance composite electrode proposes a new and feasible general pathway as 3D electrode configuration for energy storage devices.

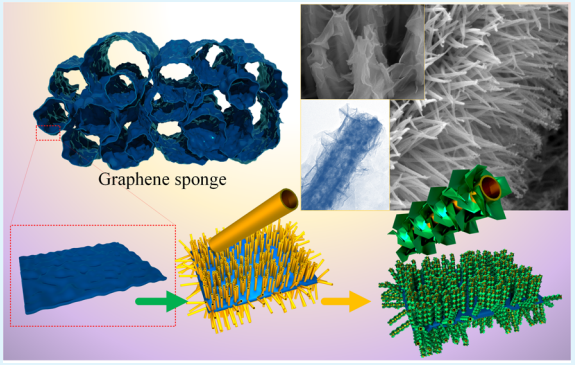

KEYWORDS: *$NiCo_2S_4$, nanotube array, graphene, supercapaitor, three-dimensional*

INTRODUCTION

Developing high-performance electrochemical energy storage devices has been one of the important issues in the energy strategic projects established by the governments of the countries around the world.[1−4] Among various energy storage devices, rechargeable supercapacitors (SCs), with high power density, fast charge–discharge rate, and long lifespan, are considered typically as one of the most appropriate choice energy storage and conversion devices.[5−9] Especially, flexible SCs, such as fiber supercapacitors,[10] all-solid-state flexible supercapacitor,[11,12] and flexible micro-supercapacitor,[13,14] have devoted a significant amount of effort, owing to their potential applications in the fields of portable electronic devices.[15,16] Nevertheless, to achieve flexible supercapacitors with the comprehensive advantage requirements, such as high charge storage capability and mechanical flexibility are the greatest challenge.[17] One of the most effective ways is to realize the perfect combination of bendable current collectors with good mechanical flexibility and electrode materials with a high capacitive performance.[18]

On the one hand, three-dimensional (3D) graphene frameworks capability of materials being formed into electrode configuration have been widely investigated in many energy storage systems, which implement fast ion and charge transport on account of their rich porosity and good conductive networks.[9,19] So far, 3D graphene network as conductive substrate obtained by several alternative technologies, such as chemical vapor deposition (CVD),[20,21] template growth,[22] self-assembly,[23,24] has been developed for supercapacitor electrode. For instance, 3D graphene foam by CVD grown cobalt oxide nanowire arrays forms a composite electrode, which delivers high C_{sp} of ∼1100 F g^{-1} at 10 A g^{-1}.[25] The surface of 3D graphene from Ni foam as template coupled a novel comb-like $CoMoO_4$,[26] which exhibited excellent C_{sp} as high as 2741 F g^{-1} at 1.43 A g^{-1} with excellent cycling stability. However, the reported 3D graphene generally have the deficiencies of irreversibly deformation under mechanical deformations. Meanwhile, large-scale manufacturing of 3D graphene is still prohibitively expensive based on the above method. Therefore, it is very significant to synthesis 3D graphene foams with favoable electrical properties and mechanical integrity requirement adopting a simple and cost-effective synthetic route.

On the other hand, the one-dimensional (1D) unique core/shell heterostructure nanoarray can be used as an ideal unit to optimize the high electrochemical performance 3D structure electrode, which improves loading mass of the active materials and provides more efficient ion contact angle between electrolyte and electrode.[27−29] For example, MnO_2/Mn/MnO_2 sandwich-like nanotube (the metal Mn layers as conducting cores) arrays have 955 F g^{-1} at 1.5 A g^{-1}.[30] A

Received: April 8, 2015
Accepted: June 30, 2015
Published: June 30, 2015

DOI: 10.1021/acsami.5b03042
ACS Appl. Mater. Interfaces 2015, 7, 15840−15847

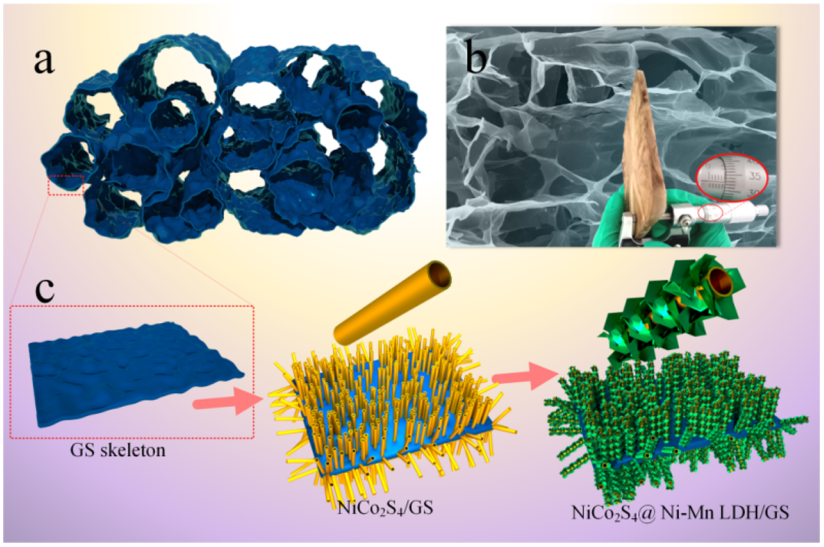

Figure 1. Process for grown 3D hierarchical configuration. (a) The principle diagram of 3D graphene oxide sponge. (b) SEM image and Physical map (inserted in) of graphene oxide sponge. (c) Schematic diagram illustrating the fabrication processes for growth $NiCo_2S_4$ nanotube@Ni−Mn LDH arrays on GS.

Ni_3S_2@$Ni(OH)_2$/3D graphene electrode, the Ni_3S_2 nanorods as both active material and charge transfer core, exhibits high Csp of 1037.5 F g^{-1} at 5.1 A g^{-1}.[31] 3D CoO@polypyrrole nanowire arrays (the role of CoO nanowire similar to above Ni_3S_2 nanorods) lead to 2223 F g^{-1}.[32] $NiCo_2S_4$ not only possessed a high Csp and excellent cycle life, but also exhibited conductivity ∼100 times of $NiCo_2O_4$.[33,34] In this sense, 1D $NiCo_2S_4$ nanotube is considered to be an excellent skeleton material for loading active materials. In addition, Ni−Mn layer double hydroxide (Ni−Mn LDH), with both Ni and Mn ions, Ni−Mn hydroxide can offer richer redox reactions roughly the same way as Ni−Co layered double hydroxides than the corresponding single component hydroxides.[35−37] For example, NiMn-LDH/carbon nanotube delivers 2960 F g^{-1} at 1.5 A g^{-1}, excellent cyclic stability.[38] As a consequence, this maybe offers a unique opportunity to construct a brilliant electrode for maximum specific area and favorable electrode/solution contact angle.

Herein, we first fabricated a novel 3D $NiCo_2S_4$ nanotube@Ni−Mn layered double hydroxide arrays in situ grown on graphene sponge hierarchical network architectures (3D $NiCo_2S_4$@Ni−Mn LDH/GS). Notably, the 3D graphene sponge was obtained from a colloidal dispersion of graphene oxide using a simple directional freeze-drying technique which has rich porosity, high specific surface area, fast electronic conductivity, and ionic conductivity suitable for as a basal growth. The high conductive $NiCo_2S_4$ nanotube not only shows excllent pseudocapacity, but also useful as a conductive support for high-performance Ni−Mn double hydroxide. As-obtained 3D $NiCo_2S_4$@Ni−Mn LDH/GS shows a high Csp and good Stability. To further evaluate the potential application of the $NiCo_2S_4$@Ni−Mn LDH arrays/GS electrode electrode in supercapacitors, a flexible asymmetric supercapacitor (FASC, $NiCo_2S_4$ nanotube@Ni−Mn LDH arrays/GS//VN/GS) was fabricated in 6 M KOH. The FASC has demonstrated high energy density and high power density.

EXPERIMENTAL SECTION

Preparation of Graphene Oxide Sponge. A colloidal dispersion of graphene oxide was prepared by oxidizing natural graphite powders based on the modified Hummers method.[39,40] The resulting viscous graphene oxide dispersion solution was sonicated for 30 min. The viscous dispersion solution was then freeze-dried using a lyophilizer (LGJ-18 vacuum freeze-dryer) for 1 day and obtained graphene oxide sponge (GOS).

Fabrication of the $NiCo_2S_4$ Nanotube@Ni−Mn LDH Arrays Grown on GS. The Ni−Mn LDH@$NiCo_2S_4$ nanotube arrays/GS were prepared by multistep hydrothermal reaction. First, Ni−Co-salt precursor nanowire arrays were grown on graphene sponge. A 60 mL mix solution containing 6 mmol $CoCl_2$, 3 mmol $NiCl_2$, and 10 mmol urea in distilled water was transferred into a 100 mL Teflon-lined stainless steel. Then the graphene sponge was immersed into the mix solution and hydrothermally treated at 120 °C for 10 h. The samples were collected and washed with deionized water and ethanol several times. Second, $NiCo_2S_4$ nanotube arrays/GS were obtained. The obtained Ni−Co-salt precursor nanowire arrays/GS was immersed into a 60 mL solution containing 300 mg $Na_2S{\cdot}9H_2O$ in distilled water. And then it was transferred into 100 mL Teflon-lined stainless steel autoclave at 180 °C for 6 h and. The $NiCo_2S_4$ nanotube arrays/GS was collected and washed with deionized water and ethanol several times after drying.

Fabrication of the $NiCo_2S_4$ Nanotube@Ni−Mn LDH Arrays Grown on GS. A 30 mL mix solution containing 3 mmol $NiCl_2$, 1 mmol $MnCl_2$ and 5 mmol hexamethylenetetramine (HMT) was transferred into a 100 mL Teflon-lined stainless steel autoclave. Then the as-obtained $NiCo_2S_4$ nanotube arrays/GS was immersed into the mix solution and maintained at 90 °C for 6 h. Finally, the $NiCo_2S_4$@Ni−Mn LDH arrays/GS was obtained by washed, vacuum-dried overnight.

Assembly of Asymmetric $NiCo_2S_4$ @Ni−Mn LDH/GS//VN/GS Capacitors. A cellulose film was used as a separator between $NiCo_2S_4$ @Ni−Mn LDH/GS cathodes and VN/GS anodes of 15 mm × 30 mm rectangular pieceswith 6.0 M KOH as electrolyte. Then we covered them in aluminum-laminated film as package and sealed the film by heating under weak vacuum. The cell was fabricated.

Materials Characterization. The phase was characterized by X-ray diffraction (XRD) (Philips X'Pert PRO; Cu Kα, λ = 0.1542 nm). The morphology of the samples was observed by FEI Quanta 200 scanning electron microscope (SEM). The structures of nanotube and nanosheet shell were investigated by means of transmission electron microscopy (TEM, JEM 2100F STEM/EDS). The X-ray photoelectron spectroscopy (XPS) spectra were measured on Kratos AXIS Ultra DLD-600W XPS system equipped with a monochromatic Al Kα (1486.6 eV) as X-ray source.

DOI: 10.1021/acsami.5b03042
ACS Appl. Mater. Interfaces 2015, 7, 15840−15847

Electrochemical Measurements. The electrochemical properties of the samples were tested with cyclic voltammetry (CV) and galvanostatic charge−discharge technique by a three-electrode system using CHI 660E electrochemical station. The 6 M KOH, Hg/HgO, and platinum plate were used as electrolyte, reference electrode, and counter, respectively. The Ni−Mn LDH@$NiCo_2S_4$ nanotube arrays/GS of 1.2 cm in diameter was applied as working electrode. The performances of the asymmetric supercapacitor were performed in a two-electrode system with CHI 660E electrochemical station. The operating current density was calculated based on the area of active materials, that is, the area of $NiCo_2S_4$@ Ni−Mn LDH arrays/GS for the three-electrode system and the total area of asymmetric flexible device ($NiCo_2S_4$@ Ni−Mn LDH arrays/GS//VN nanosheet arrays/GS) for the two-electrode system.

RESULTS AND DISCUSSION

Figure 1 illustrates the structure of graphene sponge (GS) and the fabrication processes for growth $NiCo_2S_4$ nanotubes@Ni−Mn LDH on GS. First, 3D graphene oxide sponge was obtained from a colloidal dispersion of graphene oxide using directional freeze-drying technique. The principle diagram of 3D graphene oxide sponge displayed that the thickness of the graphene oxide sponge was about 5.33 mm (Figure 1b). The 3D graphene oxide, similar to sponge (the picture as shown in Supporting Information Figure S1a), had a well-defined and interconnected 3D porous network (Figure 1b) of its freeze-dried sample. The pore walls of the graphene sponge consist of thin layers of stacked graphene sheets. Second, high conductivity $NiCo_2S_4$ nanotubes grown on GS were obtained from a Ni−Co− precursor nanorods (the SEM and TEM images as shown in Supporting Information Figure S2) sacrificial template based on Kirkendall effect.[41] The $NiCo_2S_4$ nanotubes still keep the well-ordered arrangement structure on the GS. The $NiCo_2S_4$ nanotube arrays were grown on the 3D GS network. Finally, $NiCo_2S_4$ nanotubes@ Ni−Mn Layered double hydroxide (Ni−Mn LDH) array/GS was obtained through the growth of Ni−Mn LDH nanosheets produced by hydrothermal process under 90 °C. The excellent electrochemical performances of the composite material benefit from its special 3D open configuration, which can effectively buffer the ion adsorption/desorption process.

The XRD patterns of as prepared Ni−Mn LDH/GS, $NiCo_2S_4$/GS, and $NiCo_2S_4$ nanotube@Ni−Mn LDH arrays/GS are show in Figure 2. The XRD spectrum of the as-grown $NiCo_2S_4$ nanotube@Ni−Mn LDH arrays/GS shows peaks at 2θ = 26.8, 29.9, 31.5, 38.1, 47.4, 52.1, and 55.2, which correspond to the $NiCo_2S_4$ (Supporting Information Figure S3). It should be noted that four characteristic peaks for hydrotalcite-like phase at 2θ = at 12.1°, 24.4°, 33.3°, and 59.5°. The XRD pattern of Ni−Mn LDH/GS can be indexed to a rhombohedral LDH phase, which possess interbrucite-like sheet distances (d_{003}) of 7.75 Å.[38] While the presence of the graphene was not clearly confirmed by the XRD pattern, possibly due to too much weak to obvious, it was confirmed from the HRTEM image.

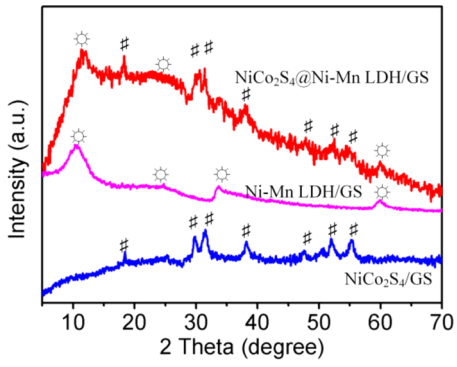

Figure 2. XRD pattern of the Ni−Mn LDH/GS, $NiCo_2S_4$/GS, and $NiCo_2S_4$@ Ni−Mn LDH/GS.

The morphologies of the $NiCo_2S_4$ nanotube/GS and $NiCo_2S_4$ nanotube@Ni−Mn LDH on graphene sponge are shown in Figure 3. Figure 3a and b show the as-formed

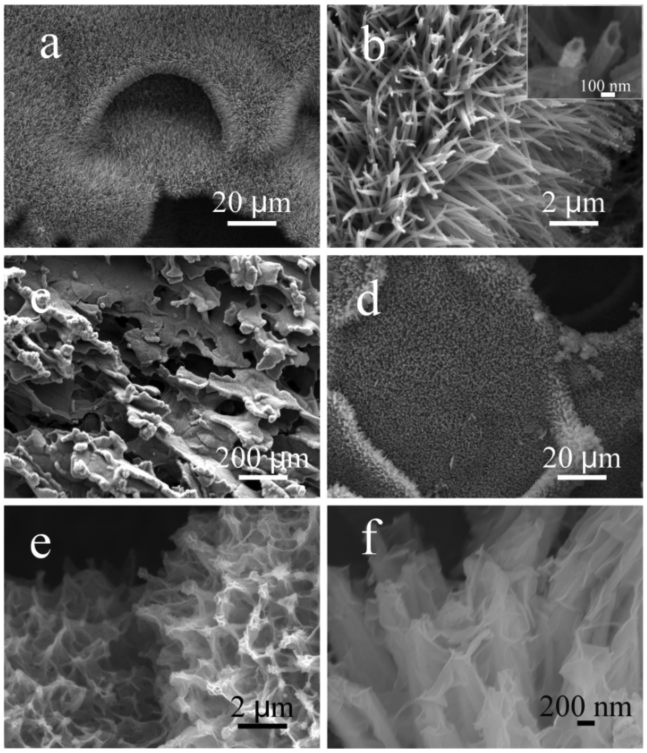

Figure 3. (a, b) $NiCo_2S_4$ nanotube/GS (high magnification image inserted in panel b). (c−f) $NiCo_2S_4$ nanotube@Ni−Mn LDH arrays/GS at different magnifications.

$NiCo_2S_4$ nanotube with ~5 μm in length are uniformly grown on the graphene sponge skeleton. In this structure, 3D graphene sponge simultaneously acts as a growth substrate and current collector for $NiCo_2S_4$ nanotube arrays. Noteworthily, the microstructure of $NiCo_2S_4$ nanotube@Ni−Mn LDH arrays/GS inherited the porous interconnected network of 3D graphene. The special interconnected network structure not only provides a convenient ion diffusion channel, but also increases more efficient contact between the ions and the active material. Both of them are seen as promising electrode materials for supercapacitors. Figure 3c and d clearly display the well-established texture structure of the $NiCo_2S_4$@Ni−Mn LDH core−shell grown on the graphene sponge. Comparing to the smooth surface of the $NiCo_2S_4$ (as shown in Figure 3b), Figure 3e and f indicate that Ni−Mn nanosheets are grown on the surface of the $NiCo_2S_4$ nanotubes, forming core/shell architecture, indicating the intimate interface contact between Ni−Mn OH nanosheet shells and $NiCo_2S_4$ nanotube cores, which could play an important role in improving the electrochemical performance. The cross-sectional SEM images (Supporting Information Figure S5a and S5b) indicate that the

DOI: 10.1021/acsami.5b03042
ACS Appl. Mater. Interfaces 2015, 7, 15840−15847

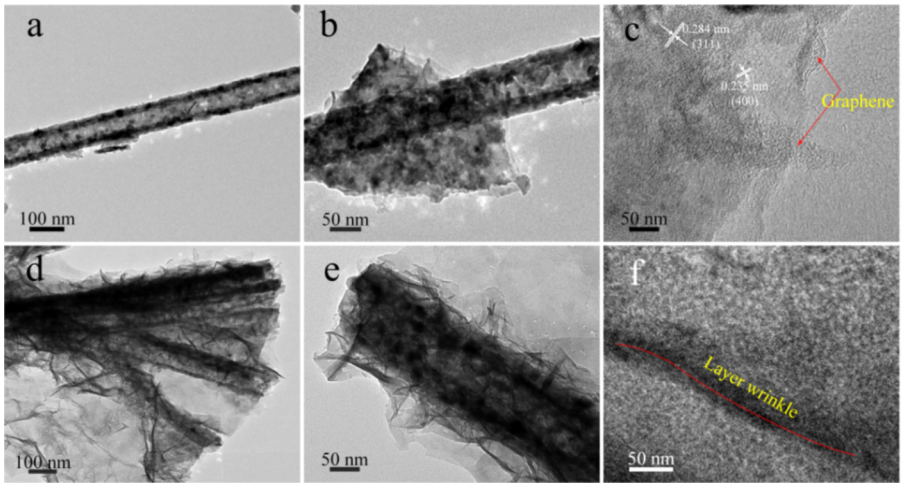

Figure 4. Low and high magnification TEM images of (a–c) the $NiCo_2S_4$ nanotubes. (d–f) $NiCo_2S_4$@Ni–Mn LDH.

Ni–Mn LDH nanosheets are homogeneously covered the whole surface of the $NiCo_2S_4$ nanotubes. This nanotube@nanosheet array could reveal excellent electrochemical performance owing to its effectively ion diffusion channel and fast electron conduction during adsorption/desorption process.

More detailed structural information and morphology evolution of the $NiCo_2S_4$ nanotube@Ni–Mn LDH arrays/GS were investigated by TEM. The typical TEM images of $NiCo_2S_4$ nanotubes in Figure 4a and b show that the diameter of $NiCo_2S_4$ nanotube is confirmed to be about 100 nm, and the wall thickness is estimated to be about 25 nm. The measured lattice spacings of 0.284 and 0.235 nm in HRTEM image of Figure 4c are corresponding to the (311) and (400) planes of cubic $NiCo_2S_4$, respectively. Most notably, the $NiCo_2S_4$ nanotubes can be in situ together with graphene skeleton as shown in Figure 4b and c, which could provide fast charge transfer pathways for high rate charge–discharge. The TEM images (Figure 4d and e) taken from the $NiCo_2S_4$ nanotube@Ni–Mn LDH confirm that the surfaces of $NiCo_2S_4$ nanotubes are uniformly coated with a layer of Ni–Mn LDH nanosheets. Figure 4f clearly shows the thin layer is a few stack folds; this kind of stretch structure is more advantageous to ion diffusion during electrochemical process.

X-ray photoelectron spectroscopy (XPS) was utilized to analyze the composition information on the $NiCo_2S_4$ nanotube@Ni–Mn LDH arrays/GS (Figure 5). The compositional elements of the composite identified from the full survey scan XPS spectrum (Figure 5a). Th Ni 2p spectrum can be deconvoluted into two spin–orbit doublets and two shakeup satellites (Figure 5b). The first doublet at 853.1 and 871 eV and the second at 854.8 and 873.2 eV could be assigned to Ni^{2+} and Ni^{3+}, corresponding to a 2p level splitting of 17.9 and 18.6 eV, respectively.[42,43] The third Ni $2p_{3/2}$ component located at 860.1 eV is related to a shakeup satellite of Ni^{3+} species. The Co $2p_{3/2}$ part of the Co 2p spectrum was fitted using three components as well. The Co $2p_{3/2}$ component observed at 778.2 is attributed to Co^{3+} species, while the components located at 781.3 and 786.4 eV correspond to Co^{2+} main peak accompanied by its shakeup satellite, respectively (Figure 5c). Mn 2p spectrum region (Figure 5d) demonstrates two peaks at 642.2 and 655.3 eV originated from Mn $2p_{3/2}$ and Mn $2p_{1/2}$ spin–orbit peaks, respectively, indicating that element Mn is Mn (III).[44] The binding energies at 166.6 and 162.1 eV correspond to S $2p_{1/2}$ and S $2p_{3/2}$, respectively (Figure 5e).

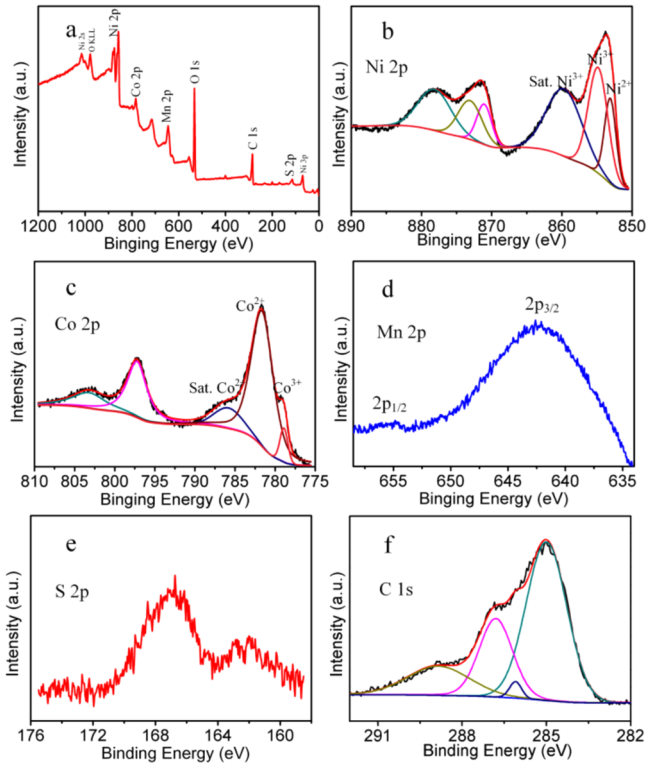

Figure 5. XPS spectra of $NiCo_2S_4$ nanotube@Ni–Mn LDH arrays/GS, (a) The survey XPS spectrum, (b) Ni 2p, (c) Co 2p, (d) Mn 2p, (e) S 2p, and (f) C 1s.

From the deconvoluted XPS peaks of C 1s (Figure 5f), it is found that four peaks (287.6, 286.3, 285.2, and 284.8 eV) which were assigned to C–O–C, C–OH, C–O, and C=C, respectively, suggesting that there are still some residual oxygen-containing functionalities on the surface of graphene networks.[45,46]

Electrochemical Characterization of Electrodes. The CV curves of the Ni–Mn LDH/GS, $NiCo_2S_4$/GS, and $NiCo_2S_4$ nanotube@Ni–Mn LDH arrays/GS recorded at 10 mV s^{-1} was shown in Figure 6a. All of the CV curves possess two pairs of redox peaks, which indicate the electrochemical process imply the presence of reversible Faradaic reaction. The above Faradaic process also can be verified from the triangle shape

DOI: 10.1021/acsami.5b03042
ACS Appl. Mater. Interfaces 2015, 7, 15840–15847

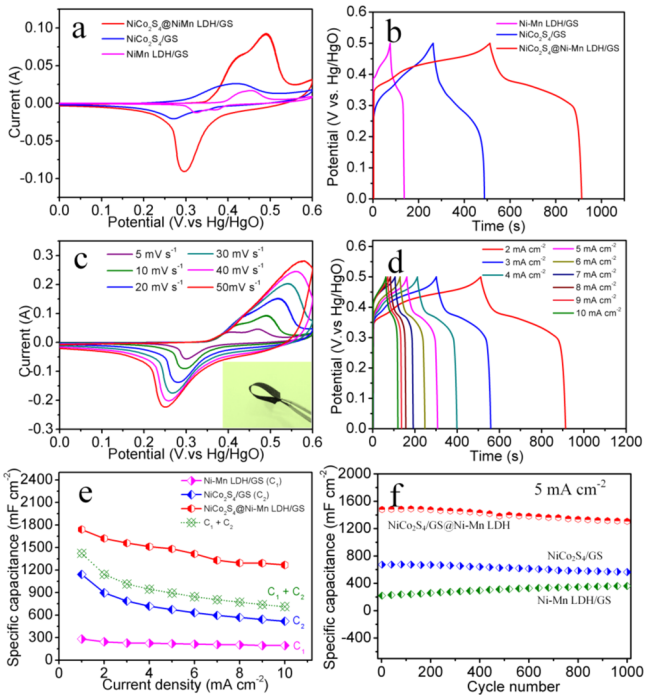

Figure 6. (a) CV and (b) galvanostatic charge–discharge curves of Ni–Mn LDH/GS, $NiCo_2S_4$/GS and $NiCo_2S_4$ @Ni–Mn LDH arrays/GS. (c) CV and (d) galvanostatic charge–discharge curves of $NiCo_2S_4$@Ni–Mn LDH arrays/GS. (e) C_{sp} as a function of current densities. (f) Cycling life at 5 mA/cm^{-2} (1000 cycles).

of the galvanostatic charge–discharge curves at 2 mA cm^{-2} in Figure 6b. Furthermore, the Csp of the $NiCo_2S_4$ nanotube@Ni–Mn LDH arrays/GS calculated from CV curves and charge/discharge curves, which is higher than Ni–Mn LDH/GS and $NiCo_2S_4$/GS. Figure 6c shows the CV curves of the $NiCo_2S_4$ nanotube@Ni–Mn LDH arrays/GS electrode at different scan rates, which display two pairs of redox peaks. With one pair of redox peaks, the potentials of the redox processes of Co^{2+}/Co^{3+} and Mn^{4+}/Mn^{3+}[44] are coincident. The other a pair of redox peaks, the potentials of the redox processes of Co^{3+}/Co^{4+} and Ni^{2+}/Ni^{3+}[41,47] are characteristic of reversible faradaic redox reactions. In addition, the picture inserted in Figure 6c shows that our $NiCo_2S_4$ nanotube@Ni–Mn LDH arrays/GS electrode possesses good flexibility. The Csp (areal capacitance) of the flexibility electrode was calculated from the following equation: $C_{sp} = I\Delta t/\Delta VS$, where I is the discharge current (A), Δt is the discharge time (s), ΔV is the voltage drop upon discharging (V), and S is the area of electrode (cm^{-2}), respectively. Figure 6d shows the galvanostatic discharge curves of the electrode at different current densities. A high Csp 1740 mF cm^{-2} was obtained at a discharge current density of 1 mA cm^{-2}. Even at a relatively high current density of 10 mA cm^{-2}, a Csp of 1135 mF cm^{-2} was obtained. That is higher than most of the literature on performance, such as, Co_3O_4 nanowire@MnO_2 ultrathin nanosheet arrays (700 mF cm^{-2}),[48] Co_3O_4 porous nanowall (0.52 F cm^{-2} at 3.2 mA cm^{-2})[49] and nanowires (1.5 F cm^{-2} at 5 mA cm^{-2}),[50] Fe_3O_4–SnO_2 core–shell nanorodfilm (7 mF cm^{-2}).[51] The Csp and retention rate of three electrodes are shown in Figure 6e, respectively. The $NiCo_2S_4$ nanotube@Ni–Mn LDH arrays/GS demonstrated evidently higher C_{sp} values and better rate capabilities than Ni–Mn LDH/GS and $NiCo_2S_4$/GS. Particularly, the C_{sp} of the $NiCo_2S_4$ nanotube@Ni–Mn LDH arrays/GS is higher than the sum of the Ni–Mn LDH/GS (C1) and $NiCo_2S_4$/GS (C2). It may be a large number of $NiCo_2S_4$ nanotube array on the grapheme sponge provide more growing point than smooth graphene skeleton for Ni–Mn LDH nanosheets. So, the Csp of the $NiCo_2S_4$ nanotube@Ni–Mn LDH arrays/GS is the biggest of all. In addition, the Csp of $NiCo_2S_4$@Ni–Mn LDH/GS demonstrated evidently higher values than Ni–Mn LDH/GS and $NiCo_2S_4$/GS according to the massed of whole electrodes as shown in Supporting Information Figure S6. We measured the charge transport and ion diffusion of two-electrode materials using electrochemical impedance spectroscopy, from which their Nyquist plots were generated as show in Supporting Information Figure S7. The ESR of $NiCo_2S_4$@ Ni–Mn LDH/GS electrode is lower than Ni–Mn LDH/GS due to $NiCo_2S_4$ nanotube providing electronic conduction for Ni–Mn LDH. Warburg resistance of $NiCo_2S_4$@ Ni–Mn LDH/GS electrode

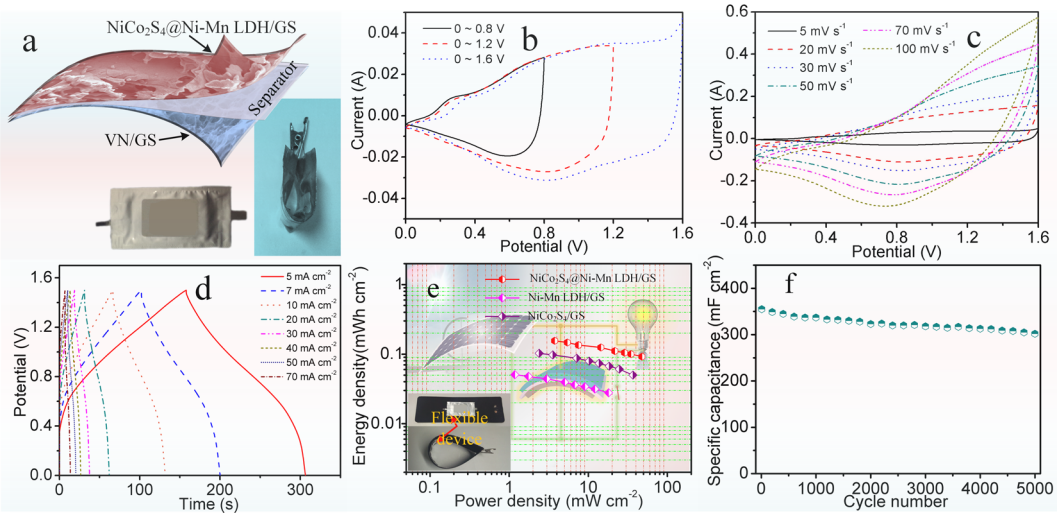

Figure 7. (a) Schematic illustration of the FASC configuration. (b) CV curves of FASC collected in different scan voltage windows at 5 mV s^{-1}. (c) CV and (d) discharge curves of the FASC. (e) Ragone plot, the working principle diagram of the flexible components was inserted. (f) Cycling stability of the FASC.

DOI: 10.1021/acsami.5b03042
ACS Appl. Mater. Interfaces 2015, 7, 15840–15847

is lower than Ni−Mn LDH/GS, $NiCo_2S_4$/GS, which indicate that the $NiCo_2S_4$@ Ni−Mn LDH/GS composite electrode possess ionic conductivity suitable. The cycling performances of the $NiCo_2S_4$ nanotube@Ni−Mn LDH arrays/GS, Ni−Mn LDH/GS and $NiCo_2S_4$/GS at 5 mA cm^{-2} are shown in Figure 6f. The C_{sp} of the $NiCo_2S_4$ nanotube@Ni−Mn LDH arrays/GS has 1307 mF cm^{-2} (88.3% of the initial value of 1480 mF cm^{-2}) after 1000 cycles.

Electrochemical Characterization of Asymmetric Supercapacitor. To further assess the potential application of the $NiCo_2S_4$ nanotube@Ni−Mn LDH arrays/GS electrode electrode in supercapacitors, a flexible asymmetric supercapacitor (FASC, $NiCo_2S_4$ nanotube@Ni−Mn LDH arrays/GS//VN/GS) was fabricated and investigated by two-electrode device using the $NiCo_2S_4$ nanotube@Ni−Mn LDH arrays/GS electrode as positive electrode and the vanadium nitride/graphene sponge (the preparation process of VN/GS inside the Supporting Information, the XRD pattern and SEM in Supporting Information Figure S8, CV curves and galvanostatic charge−discharge curves in Supporting Information Figure S9) as negative electrode in 6 M KOH according to befitting weight ratio of positive and negative electrodes (Supporting Information Figure S10). Figure 7a displays the schematic illustration of the structure for the FASC, the picture of the flexible packaged device was inserted.

Figure 7b shows the CV curves of the FASC at different voltage windows, an operating cell voltage from 0.8 to 1.6 V, which indicates the stable working potential of the FASC can achieve 1.6 V. Figure 7c shows a pair of strong peaks from the CV curves of the device under different scan rates from 5 to 100 mV s^{-1}, corresponding to the typical faradaic pseudocapacitive of the single electrode $NiCo_2S_4$ nanotube@Ni−Mn LDH arrays/GS. Galvanostatic discharge curves of the FASC at a set of current densities of 5−70 mA cm^{-2} were further illustrated in Figure 7d. The discharge areal capacitance of the FASC has 495 mF cm^{-2} at 5 mA cm^{-2}, still keeping 321 mF cm^{-2} at 70 mA cm^{-2}. We test CV curves and discharge curves of the device after bending at 5 mV s^{-1} and 2 mA cm^{-2}, respectively, as shown in Supporting Information Figure S11. The FASC keeps a good capacitance performance after 50th bending. Ragone plot (power density vs energy density) of the FASC describing was obtained and shown in Figure 7e. The energy density decreased from 0.156 to 0.09 mWh cm^{-2}, compared to the power density increased from 3.76 to 47.7 mW cm^{-2}, as the discharge current density increased from 5 to 70 mA cm^{-2}, which is substantially higher than the other two FASCs, Ni−Mn LDH/GS//VN/GS and $NiCo_2S_4$/GS//VN/GS. The cycling stability of the FASC was further investigated by virtue of galvanostatic charge/discharge cycling between 0 and 1.5 V at 20 mA cm^{-2} (as shown in Figure 7f). The C_{sp} retained 84.5% after 5000 cycles, indicating its good cycle stability. Supporting Information Figure S12b shows the LED working with flexible solar cells under the light; Supporting Information Figure S12d displays LED still working with flexible solar cells at the dark, while the FASC power supply for the system. The outstanding capacitive performances of the device originate from high C_{sp} of electrodes (as well as good quality match of the positive and negative electrodes), high working voltage of the asymmetric supercapacitor.

CONCLUSION

We fabricated a novel 3D $NiCo_2S_4$ nanotube@Ni−Mn LDH arrays in situ grown on graphene sponge hierarchical network configuration. The 3D graphene sponge has obtained using a simple directional freeze-drying technique, which can be used as an accessible big channel and large mass loading of flexible conductive substrate for the growth of $NiCo_2S_4$ nanotube@ Ni−Mn LDH arrays. The high conductive $NiCo_2S_4$ nanotube shows excellent pseudocapacity and is used as a good conductive support for high-performance Ni−Mn LDH. The high capability flexible $NiCo_2S_4$ nanotube@ Ni−Mn LDH arrays/GS electrode is an ideal of flexible supercapacitor electrode. A flexible asymmetric supercapacitor ($NiCo_2S_4$ nanotube@Ni−Mn LDH arrays/GS//VN/GS) has demonstrated high energy density and high power density. Therefore, our work not only opens up a high-performance composite flexible electrode based on large-scale preparation of graphene by a simple and low energy consumption freeze-dried technique, but also proposes a new and feasible general method as 3D electrode configuration for energy storage systems.

ASSOCIATED CONTENT

Supporting Information

SEM images of three-dimensional structures and XRD pattern and SEM images of the VN/graphene. Electrochemical performances of the VN/graphene. The Supporting Information is available free of charge on the ACS Publications website at DOI: 10.1021/acsami.5b03042.

AUTHOR INFORMATION

Corresponding Author

*E-mail: jiangjj@mail.hust.edu.cn. Tel.: +86-27-87544472. Fax: +86-27-87544472.

Notes

The authors declare no competing financial interest.

ACKNOWLEDGMENTS

This work was supported by the National Natural Science Foundation of China (51302097) and Wuhan Planning Project of Science and Technology (2013011801010594). The authors thank to the Analytical and Testing Center of Huazhong University of Science and Technology for support. We thank T. T. Luo from the Testing Center of Wuhan University of Technology for characterization and discussions.

REFERENCES

(1) Xie, K.; Wei, B. Materials and Structures for Stretchable Energy Storage and Conversion Devices. *Adv. Mater.* **2014**, *26*, 3592−3617.

(2) Baxter, J.; Bian, Z.; Chen, G.; Danielson, D.; Dresselhaus, M. S.; Fedorov, A. G.; Fisher, T. S.; Jones, C. W.; Maginn, E.; Kortshagen, U.; Manthiram, A.; Nozik, A.; Rolison, D. R.; Sands, T.; Shi, L.; Sholl, D.; Wu, Y. Nanoscale Design to Enable the Revolution in Renewable Energy. *Energy Environ. Sci.* **2009**, *2*, 559−588.

(3) Xu, J.; Wang, Q.; Wang, X.; Xiang, Q.; Liang, B.; Chen, D.; Shen, G. Flexible Asymmetric Supercapacitors Based upon Co_9S_8 Nanorod//Co_3O_4@RuO_2 Nanosheet Arrays on Carbon Cloth. *ACS Nano* **2013**, *7*, 5453−5462.

(4) Xiao, X.; Li, T.; Peng, Z.; Jin, H.; Zhong, Q.; Hu, Q.; Yao, B.; Luo, Q.; Zhang, C.; Gong, L.; Chen, J.; Gogotsi, Y.; Zhou, J. Freestanding Functionalized Carbon Nanotube-Based Electrode for Solid-State Asymmetric Supercapacitors. *Nano Energy* **2014**, *6*, 1−9.

(5) Fan, Z.; Yan, J.; Wei, T.; Zhi, L.; Ning, G.; Li, T.; Wei, F. Asymmetric Supercapacitors Based on Graphene/MnO_2 and Activated Carbon Nanofiber Electrodes with High Power and Energy Density. *Adv. Funct. Mater.* **2011**, *21*, 2366−2375.

DOI: 10.1021/acsami.5b03042
ACS Appl. Mater. Interfaces 2015, 7, 15840−15847

(6) Su, F.; Lv, X.; Miao, M. High-Performance Two-Ply Yarn Supercapacitors Based on Carbon Nanotube Yarns Dotted with Co_3O_4 and NiO Nanoparticles. *Small* **2015**, *11*, 854−61.
(7) Cai, D.; Huang, H.; Wang, D.; Liu, B.; Wang, L.; Liu, Y.; Li, Q.; Wang, T. High-Performance Supercapacitor Electrode Based on The Unique ZnO@Co_3O_4 Core/Shell Heterostructures on Nickel Foam. *ACS Appl. Mater. Interfaces* **2014**, *6*, 15905−15912.
(8) Zhu, Y.; Murali, S.; Stoller, M. D.; Ganesh, K. J.; Cai, W.; Ferreira, P. J.; Pirkle, A.; Wallace, R. M.; Cychosz, K. A.; Thommes, M.; Su, D.; Stach, E. A.; Ruoff, R. S. Carbon-Based Supercapacitors Produced by Activation of Graphene. *Science* **2011**, *332*, 1537−1541.
(9) Lei, Y.; Li, J.; Wang, Y.; Gu, L.; Chang, Y.; Yuan, H.; Xiao, D. Rapid Microwave-Assisted Green Synthesis of 3D Hierarchical Flower-Shaped $NiCo_2O_4$ Microsphere for High-Performance Supercapacitor. *ACS Appl. Mater. Interfaces* **2014**, *6*, 1773−1780.
(10) Fu, Y.; Cai, X.; Wu, H.; Lv, Z.; Hou, S.; Peng, M.; Yu, X.; Zou, D. Fiber Supercapacitors Utilizing Pen Ink for Flexible/Wearable Energy Storage. *Adv. Mater.* **2012**, *24*, 5713−5718.
(11) Wang, K.; Zou, W.; Quan, B.; Yu, A.; Wu, H.; Jiang, P.; Wei, Z. An All-Solid-State Flexible Micro-Supercapacitor on a Chip. *Adv. Energy Mater.* **2011**, *1*, 1068−1072.
(12) Sun, H.; You, X.; Deng, J.; Chen, X.; Yang, Z.; Chen, P.; Fang, X.; Peng, H. A Twisted Wire-Shaped Dual-Function Energy Device for Photoelectric Conversion and Electrochemical Storage. *Angew. Chem., Int. Ed.* **2014**, *53*, 6664−6668.
(13) Si, W.; Yan, C.; Chen, Y.; Oswald, S.; Han, L.; Schmidt, O. G. On Chip, All Solid-State and Flexible Micro-Supercapacitors with High Performance Based on Mnox/Au Multilayers. *Energy Environ. Sci.* **2013**, *6*, 3218−3223.
(14) El-Kady, M. F.; Kaner, R. B. Scalable Fabrication of High-Power Graphene Micro-Supercapacitors for Flexible and On-Chip Energy Storage. *Nat. Commun.* **2013**, *4*, 1475−1483.
(15) He, Y.; Chen, W.; Li, X.; Zhang, Z.; Fu, J.; Zhao, C.; Xie, E. Free standing Three-Dimensional Graphene/MnO_2 Composite Networks as Ultralight and Flexible Supercapacitor Electrodes. *ACS Nano* **2013**, *7*, 174−182.
(16) Dong, X.; Guo, Z.; Song, Y.; Hou, M.; Wang, J.; Wang, Y.; Xia, Y. Flexible and Wire-Shaped Micro-Supercapacitor Based on Ni-$(OH)_2$-Nanowire and Ordered Mesoporous Carbon Electrodes. *Adv. Funct. Mater.* **2014**, *24*, 3405−3412.
(17) Yang, X.; Zhang, F.; Zhang, L.; Zhang, T.; Huang, Y.; Chen, Y. A High-Performance Graphene Oxide-Doped Ion Gel as Gel Polymer Electrolyte for All-Solid-State Supercapacitor Applications. *Adv. Funct. Mater.* **2013**, *23*, 3353−3360.
(18) Liu, Z.; Xu, J.; Chen, D.; Shen, G. Flexible Electronics Based on Inorganic Nanowires. *Chem. Soc. Rev.* **2015**, *44*, 161−192.
(19) Yoon, J.-C.; Lee, J.-S.; Kim, S.-I.; Kim, K.-H.; Jang, J.-H. Three-Dimensional Graphene Nano-Networks with High Quality and Mass Production Capability via Precursor-Assisted Chemical Vapor Deposition. *Sci. Rep.* **2013**, *3*, 1788−1796.
(20) Worsley, M. A.; Olson, T. Y.; Lee, J. R. I.; Willey, T. M.; Nielsen, M. H.; Roberts, S. K.; Pauzauskie, P. J.; Biener, J.; Satcher, J. H.; Baumann, T. F. High Surface Area, sp^2-Cross-Linked Three-Dimensional Graphene Monoliths. *J. Phys. Chem. Lett.* **2011**, *2*, 921−925.
(21) Xiao, X.; Beechem, T. E.; Brumbach, M. T.; Lambert, T. N.; Davis, D. J.; Michael, J. R.; Washburn, C. M.; Wang, J.; Brozik, S. M.; Wheeler, D. R.; Burckel, D. B.; Polsky, R. Lithographically Defined Three-Dimensional Graphene Structures. *ACS Nano* **2012**, *6*, 3573−3579.
(22) Chen, Z.; Ren, W.; Gao, L.; Liu, B.; Pei, S.; Cheng, H. M. Three-Dimensional Flexible and Conductive Interconnected Graphene Networks Grown by Chemical Vapour Deposition. *Nat. Mater.* **2011**, *10*, 424−428.
(23) Xu, Y.; Wu, Q.; Sun, Y.; Bai, H.; Shi, G. Three-Dimensional Self-Assembly of Graphene Oxide and DNA into Multifunctional Hydrogels. *ACS Nano* **2010**, *4*, 7358−7362.
(24) Gong, Y.; Yang, S.; Liu, Z.; Ma, L.; Vajtai, R.; Ajayan, P. M. Graphene-Network-Backboned Architectures for High-Performance Lithium Storage. *Adv. Mater.* **2013**, *25*, 3979−3984.
(25) Dong, X.-C.; Xu, H.; Wang, X.-W.; Huang, Y.-X.; Chan-Park, M. B.; Zhang, H.; Wang, L.-H.; Huang, W.; Chen, P. 3D Graphene−Cobalt Oxide Electrode for High-Performance Supercapacitor and Enzymeless Glucose Detection. *ACS Nano* **2012**, *6*, 3206−3213.
(26) Yu, X.; Lu, B.; Xu, Z. Super Long-Life Supercapacitors Based on the Construction of Nanohoneycomb-Like Strongly Coupled $CoMoO_4$-3D Graphene Hybrid Electrodes. *Adv. Mater.* **2014**, *26*, 1044−1051.
(27) Wang, J.; Chao, D.; Liu, J.; Li, L.; Lai, L.; Lin, J.; Shen, Z. Ni_3S_2@MoS_2 Core/Shell Nanorod Arrays on Ni Foam for High-Performance Electrochemical Energy Storage. *Nano Energy* **2014**, *7*, 151−160.
(28) You, B.; Jiang, J.; Fan, S. Three-Dimensional Hierarchically Porous All-Carbon Foams for Supercapacitor. *ACS Appl. Mater. Interfaces* **2014**, *6*, 15302−15308.
(29) Wan, L.; Xiao, J.; Xiao, F.; Wang, S. Nanostructured (Co, Ni)-based Compounds Coated on a Highly Conductive Three Dimensional Hollow Carbon Nanorod Array (HCNA) Scaffold for High Performance Pseudocapacitors. *ACS Appl. Mater. Interfaces* **2014**, *6*, 7735−7742.
(30) Li, Q.; Wang, Z. L.; Li, G. R.; Guo, R.; Ding, L. X.; Tong, Y. X. Design and Synthesis of MnO_2/Mn/MnO_2 Sandwich-Structured Nanotube Arrays with High Supercapacitive Performance for Electrochemical Energy Storage. *Nano Lett.* **2012**, *12*, 3803−3807.
(31) Zhou, W.; Cao, X.; Zeng, Z.; Shi, W.; Zhu, Y.; Yan, Q.; Liu, H.; Wang, J.; Zhang, H. One-Step Synthesis of Ni_3S_2 Nanorod@Ni$(OH)_2$ Nanosheet Core−Shell Nanostructures on a Three-Dimensional Graphene Network for High-Performance Supercapacitors. *Energy Environ. Sci.* **2013**, *6*, 2216−2221.
(32) Zhou, C.; Zhang, Y.; Li, Y.; Liu, J. Construction of High-Capacitance 3D CoO@Polypyrrole Nanowire Array Electrode for Aqueous Asymmetric Supercapacitor. *Nano Lett.* **2013**, *13*, 2078−2085.
(33) Chen, H.; Jiang, J.; Zhang, L.; Wan, H.; Qi, T.; Xia, D. Highly Conductive $NiCo_2S_4$ Urchin-Like Nanostructuresfor High-Rate Pseudocapacitors. *Nanoscale* **2013**, *5*, 8879−8883.
(34) Liu, Y.; Zhang, J.; Wang, S.; Wang, K.; Chen, Z.; Xu, Q. Facilely Constructing 3D Porous $NiCo_2S_4$ Nanonetworks for High-Performance Supercapacitors. *New J. Chem.* **2014**, *38*, 4045−4048.
(35) Gupta, V.; Gupta, S.; Miura, N. Potentiostatically Deposited Nanostructured Co_xNi_{1-x} Layered Double Hydroxides as Electrode Materials for Redox-Supercapacitors. *J. Power Sources* **2008**, *175*, 680−685.
(36) Salunkhe, R. R.; Jang, K.; Lee, S.-w.; Ahn, H. Aligned Nickel-Cobalt Hydroxide Nanorod Arrays for Electrochemical Pseudocapacitor Applications. *RSC Adv.* **2012**, *2*, 3190−3193.
(37) Zhu, G.; Xi, C.; Shen, M.; Bao, C.; Zhu, J. Nanosheet-Based Hierarchical $Ni_2CO_3(OH)_2$ Microspheres With Weak Crystallinity For High-Performance Supercapacitor. *ACS Appl. Mater. Interfaces* **2014**, *6*, 17208−17214.
(38) Zhao, J.; Chen, J.; Xu, S.; Shao, M.; Zhang, Q.; Wei, F.; Ma, J.; Wei, M.; Evans, D. G.; Duan, X. Hierarchical NiMn Layered Double Hydroxide/Carbon Nanotubes Architecture with Superb Energy Density for Flexible Supercapacitors. *Adv. Funct. Mater.* **2014**, *24*, 2938−2946.
(39) Dikin, D. A.; Stankovich, S.; Zimney, E. J.; Piner, R. D.; Dommett, G. H.; Evmenenko, G.; Nguyen, S. T.; Ruoff, R. S. Preparation And Characterization Of Graphene Oxide Paper. *Nature* **2007**, *448*, 457−460.
(40) Ye, S.; Feng, J.; Wu, P. Deposition of Three-Dimensional Graphene Aerogel on Nickel Foam as a Binder-Free Supercapacitor Electrode. *ACS Appl. Mater. Interfaces* **2013**, *5*, 7122−7129.
(41) Wan, H.; Jiang, J.; Yu, J.; Xu, K.; Miao, L.; Zhang, L.; Chen, H.; Ruan, Y. $NiCo_2S_4$ Porous Nanotubes Synthesis via Sacrificial Templates: High-Performance Electrode Materials of Supercapacitors. *CrystEngComm* **2013**, *15*, 7649−7651.
(42) Wu, J.; Dou, S.; Shen, A.; Wang, X.; Ma, Z.; Ouyang, C.; Wang, S. One-Step Hydrothermal Synthesis of $NiCo_2S_4$−rGO as an Efficient

DOI: 10.1021/acsami.5b03042
ACS Appl. Mater. Interfaces 2015, 7, 15840−15847

Electrocatalyst for the Oxygen Reduction Reaction. *J. Mater. Chem. A* **2014**, *2*, 20990−20995.
(43) Sun, H.; Qin, D.; Huang, S.; Guo, X.; Li, D.; Luo, Y.; Meng, Q. Dye-Sensitized Solar Cells with NiS Counter Electrodes Electrodeposited by a Potential Reversal Technique. *Energy Environ. Sci.* **2011**, *4*, 2630−2637.
(44) Sun, J.; Li, W.; Zhang, B.; Li, G.; Jiang, L.; Chen, Z.; Zou, R.; Hu, J. 3D Core/Shell Hierarchies of MnOOH Ultrathin Nanosheets Grown on NiO Nanosheet Arrays for High-Performance Supercapacitors. *Nano Energy* **2014**, *4*, 56−64.
(45) Yan, J.; Sun, W.; Wei, T.; Zhang, Q.; Fan, Z.; Wei, F. Fabrication And Electrochemical Performances of Hierarchical Porous $Ni(OH)_2$ Nanoflakes Anchored on Graphene Sheets. *J. Mater. Chem.* **2012**, *22*, 11494−11502.
(46) Losurdo, M.; Bergmair, I.; Dastmalchi, B.; Kim, T.-H.; Giangregroio, M. M.; Jiao, W.; Bianco, G. V.; Brown, A. S.; Hingerl, K.; Bruno, G. Graphene as an Electron Shuttle for Silver Deoxidation: Removing a Key Barrier to Plasmonics and Metamaterials for SERS in the Visible. *Adv. Funct. Mater.* **2014**, *24*, 1864−1878.
(47) Wang, X.; Yan, C.; Sumboja, A.; Lee, P. S. High Performance Porous Nickel Cobalt Oxide Nanowires for Asymmetric Supercapacitor. *Nano Energy* **2014**, *3*, 119−126.
(48) Liu, J.; Jiang, J.; Cheng, C.; Li, H.; Zhang, J.; Gong, H.; Fan, H. J. Co_3O_4 Nanowire@MnO_2 Ultrathin Nanosheet Core/Shell Arrays: a New Class of High-Performance Pseudocapacitive Materials. *Adv. Mater.* **2011**, *23*, 2076−2081.
(49) Wu, J. B.; Lin, Y.; Xia, X. H.; Xu, J. Y.; Shi, Q. Y. Pseudocapacitive Properties of Electrodeposited Porous Nanowall Co_3O_4 Film. *Electrochim. Acta* **2011**, *56*, 7163−7170.
(50) Huang, J.; Zhu, J.; Cheng, K.; Xu, Y.; Cao, D.; Wang, G. Preparation of Co_3O_4 Nanowires Grown on Nickel Foam with Superior Electrochemical Capacitance. *Electrochim. Acta* **2012**, *75*, 273−278.
(51) Li, R.; Ren, X.; Zhang, F.; Du, C.; Liu, J. Synthesis of Fe_3O_4@ Sno_2 Core-Shell Nanorod Film and Its Application as a Thin-Film Supercapacitor Electrode. *Chem. Commun.* **2012**, *48*, 5010−5012.

DOI: 10.1021/acsami.5b03042
ACS Appl. Mater. Interfaces 2015, 7, 15840−15847